MNRAS **483,** L75–L79 (2019)
Advance Access publication 2018 November 27
doi:10.1093/mnrasl/sly223

On the discrepancy between the X-ray and UV absorption measurements of O VI in the local ISM

Efraín Gatuzz,[1,2]★ Javier A. García[3,4] and Timothy R. Kallman[5]

[1]*ESO, Karl-Schwarzschild-Strasse 2, D-85748 Garching bei München, Germany*
[2]*Excellence Cluster Universe, Boltzmannstr 2, D-85748, Garching, Germany*
[3]*Cahill Center for Astronomy and Astrophysics, California Institute of Technology, Pasadena, CA 91125, USA*
[4]*Dr. Karl Remeis-Observatory and Erlangen Centre for Astroparticle Physics, Universität Erlangen-Nürnberg, Sternwartstr 7, 96049 Bamberg, Germany*
[5]*NASA Goddard Space Flight Center, Greenbelt, MD 20771, USA*

Accepted 2018 November 23. Received 2018 November 22; in original form 2018 October 8

ABSTRACT

The total amount of O VI present in the interstellar medium (ISM) obtained via absorption measurements in UV and X-ray spectra is currently in disagreement, with the latter being significantly larger (by a factor of 10 or more) than the former. Previous works have proposed that the blend of the O VI Kα line (22.032 Å) with the O II Kβ-L12 line (22.04 Å) could account for the stronger absorption observed in the X-ray spectra. Here, we present a detailed study of the oxygen absorption in the local ISM, implementing our new model `IGMabs` which includes photoabsorption cross-sections of highly ionized species of abundant elements as well as turbulence broadening. By analysing high-resolution *Chandra* spectra of 13 low-mass X-ray binaries (LMXBs) and 29 extragalactic sources, we have estimated the column densities of O I – O III and from O VI – O VIII along multiple line-of-sights. We find that in most cases the O II Kβ-L12 line accounts for $<$30 per cent of the total O VI K α + O II K β. We conclude that the amount of O II predicted by our model is still insufficient to explain the discrepancy between X-ray and UV measurements of O VI column densities.

Key words: ISM: atoms – ISM: abundances – ISM: structure – Galaxy: structure – X-rays: ISM.

1 INTRODUCTION

The interstellar medium (ISM) is one of the most important ingredients in the star life cycles, affecting the dynamics of the Galaxy. This complex environment can be analysed by using astronomical observations from different energy bands, including optical (e.g. Welsh et al. 2010; Brandt & Draine 2012; Bailey et al. 2015; Schlafly et al. 2016), radio (e.g. Kalberla et al. 2005; Willingale et al. 2013; Anderson et al. 2015; Moss, Lockman & McClure-Griffiths 2017), infrared (e.g. Jackson et al. 2008; García et al. 2014; Giannetti et al. 2015; Xue et al. 2016), ultra-violet (UV) (e.g. Bowen et al. 2008; Wakker et al. 2012; Savage et al. 2017), and X-rays (e.g. Juett, Schulz & Chakrabarty 2004; Juett et al. 2006; Gatuzz et al. 2013; Miller & Bregman 2015; Nicastro et al. 2016b; Gatuzz & Churazov 2018; Gatuzz et al. 2018). X-ray photons, in particular, are capable of tracing multiple phases of the ISM, namely cold, warm, and hot. Given that most of the baryonic matter resides among galaxies in the warm–hot phases (Shull, Smith & Danforth 2012; McQuinn 2016), X-ray spectra constitute a useful way to measure column densities, ionization state, and abundances of the intergalactic medium (Nicastro et al. 2016b; Faerman, Sternberg & McKee 2017; Arcodia et al. 2018).

The hot component of the ISM, in particular, can be traced by O VI absorption lines in both, the UV and X-ray bands, providing a useful tool to study the abundance and ionization structure of the plasma (Pradhan 2000). However, even when the integrated O VI column density measured with UV instruments must be equal to that obtained from the X-ray data, there is a well known mismatch between both measurements with differences as large as a factor of a few up to one order of magnitude (Arav et al. 2003; Mathur et al. 2017). There are several contaminants that would affect the N(O VI) measured by UV data. For example, the 1038 Å feature is affected by C II$*$ and H_2 absorption while the 1032 Å feature is affected by H_2 and HD (Pathak et al. 2011). However, when modelling in detail such contaminants, the UV column densities become smaller, hence, creating a bigger gap between the X-ray and UV data (Sarma et al. 2017). Given that in UV the lines are resolved and unsaturated, the atomic parameters are well known, and the resulting column densities make physical sense considering the mechanisms that could produce O VI, it is unlikely for UV measurements to be inaccurate.

Recently, Mathur et al. (2017) proposed that the mismatch between column densities is due to contamination of the O VI K α

★ E-mail: efraingatuzz@gmail.com

absorption line, located at 22.032 Å (McLaughlin et al. 2017), with the O II K β 'line 12" (L12, thereafter) transition located at 22.04 Å (Bizau et al. 2015). By analysing *XMM–Newton* spectra from 23 sources, they measured equivalent widths (EWs) for the O II K α transition in order to estimate the O II K β-L12 level of contamination to the O VI K α absorption line. They concluded that the Galactic N(O VI) measured in UV is too small to be detectable in X-ray and that the 22.032 Å X-ray absorption line is almost entirely dominated by the O II K β-L12 transition. It should be noted that their conclusions are only valid for $z = 0$ systems while discrepancies at higher redshift require other explanations. We are testing this idea by performing a detailed analysis of the oxygen X-ray absorption in the local ISM along multiple line-of-sights, with emphasis on the O VI absorption features, and the influence of the O II absorption on its modelling. The outline of this report is as follows. In Section 2, we explain the data selection and data reduction processes. In Section 3, we describe and discuss the results obtained from the spectral fitting. Finally, Section 4 summarizes our main conclusions.

2 OBSERVATIONS AND FITTING PROCEDURE

In order to measure the O VI absorption in the local ISM, we used a sample of both Galactic and extragalactic sources based on the sources previously analysed by Gatuzz & Churazov (2018). We decided to exclude *XMM–Newton* observations due to the presence of instrumental features in the Reflection Grating Spectrometers (RGS; den Herder et al. 2001). These instrumental imperfections contaminate the O VI K α absorption feature at 22.032 Å, which is of central interest in this work. Thus, the final sample consists of 13 LMXBs and 29 extragalactic sources. Observations were reduced following the standard CIAO threads[1] and the zero-order position were estimated with the `findzo` algorithm.[2] For each source, all observations were combined using the `combine_grating_spectra` command. The spectral fitting was performed with the XSPEC software (version 12.9.1p[3]). Finally, we used χ^2 statistics in combination with the Churazov et al. (1996) weighting method which allows the analysis of low-counts spectra.

Gaussian profiles are commonly used in order to model X-ray absorption features associated to the ISM. However, if the analysis is focused in only one absorption line, ignoring the presence of absorption features due to other transitions of the same ion or due to the presence of different ions, the column densities can be over(under)estimated (Gatuzz et al. 2014, 2016). To address this issue, we have built a model for the entire oxygen K-shell region (18–24 Å), which includes absorption features from O I–O VIII ions. In order to fit the absorption features from the low-ionization ions O I–O III, we use the `ISMabs` model (Gatuzz et al. 2015). These ions are associated to the neutral–warm components of the ISM (Gatuzz et al. 2016; Gatuzz & Churazov 2018). Then, we developed a new model called `IGMabs`, which is similar to `ISMabs` but includes photoabsorption cross-sections from highly ionized ions, in order to model absorption features associated to O VI–O VIII ions.

Fig. 1 shows the oxygen photoabsorption cross-sections included in the present analysis. Note that, in the computation of such cross-sections, the Auger broadening can be the dominant broadening

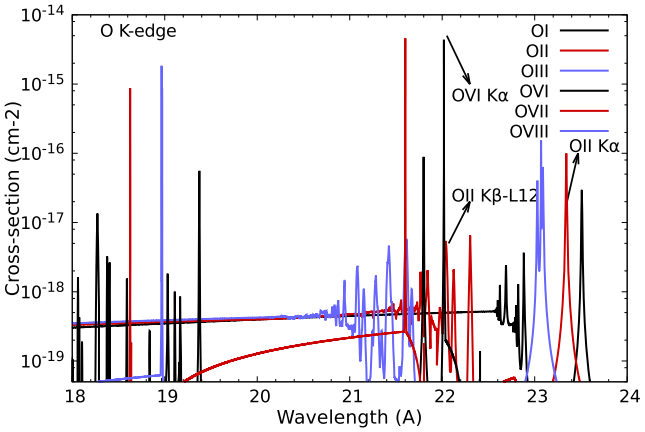

Figure 1. Oxygen photoabsorption cross-sections that are implemented in the `ISMabs` (O I–O III ions) and `IGMabs` (O VI–O VIII ions) model.

process, and is included. As the plot shows, the O VI K α resonance lies close to the O II K β-L12 transition and the cross-section is larger for the former. It is important to note that the `IGMabs` model also includes a turbulence velocity parameter $v_{\rm turb}$, which is required when modelling the hot component of the ISM. Following the analysis in Gatuzz & Churazov (2018), we have fixed the $v_{\rm turb}$ parameter of the `IGMabs` model to 60 km s^{-1} for the Galactic sources and to 110 km s^{-1} for the Extragalactic sources. Finally, for each source, we have used a `power-law` component to model the continuum and have fixed the N(H) of the `ISMabs` model to the 21 cm values from Willingale et al. (2013). In this way, the free parameters in our fitting procedure are the oxygen column densities and the `power-law` parameters.

3 RESULTS AND DISCUSSION

Table 1 shows the oxygen column densities obtained for all sources analysed. N(O VI) obtained by Savage et al. (2003) using observations from the Far Ultraviolet Spectroscopic Explorer (*FUSE*) are included for those sources for which data is available. We have found that both N(O II) and N(O VI) can be simultaneously constrained only for four sources in the sample: Cygnus X–2, XTE J1817-330, H2356–309, and Mrk 421. For the rest of the sources, we have measured upper limits for the N(O VI). We also have measured the column densities for each observation of the sources (i.e. instead of combining the spectra) and found that the N(O VI) do not vary between different observations (considering the uncertainties), pointing out to an ISM origin of the absorber. For Mrk 421, Mrk 509, and PKS 2155-304, our results are consistent with Mathur et al. (2017). Because we are modelling the complete oxygen edge absorption region, the maximum amount of N(O II) is constrained by the presence of both the K α and the K β transitions. Moreover, the contribution of the photoabsorption cross-section from the multiple ions to the continuum is not negligible. From Table 1, it is clear that there is a discrepancy with X-ray best-fit results and the UV values obtained from *FUSE* observations by Savage et al. (2003). That is, even when the N(O II) is accurately modelled, the N(O VI) estimated from X-ray observations can be up to two orders of magnitude larger than the UV measurements. Using the column densities derived with the `IGMabs` model, we have computed the EWs for the O VI K α and O II K β-L12 absorption lines. Fig. 2 shows thepercentage contribution of O II K β-L12 to the total (O VI Kα + O II K β-L12) EW. In most cases, the O II K β-L12 ac-

[1] http://cxc.harvard.edu/ciao/threads/gspec.html
[2] http://space.mit.edu/cxc/analysis/findzo/
[3] https://heasarc.gsfc.nasa.gov/xanadu/xspec/

Table 1. Best-fit results obtained for all sources included in the sample.

Source	N(H) − 21 cm (10^{21}cm^{-2})	N(O I) (10^{16}cm^{-2})	N(O II) (10^{16}cm^{-2})	N(O III) (10^{16}cm^{-2})	N(O VI) (10^{16}cm^{-2})	N(O VII) (10^{16}cm^{-2})	N(O VIII) (10^{16}cm^{-2})	N(O VI)-*FUSE* (10^{16}cm^{-2})
Galactic sources								
4U 0614 + 091	4.42	144.97 ± 0.22	5.41 ± 1.28	3.28 ± 0.67	<0.64	<0.82	<0.22	–
4U 1636-53	4.04	54.77 ± 0.16	<4.17	<6.42	<0.62	1.57 ± 0.50	1.02 ± 0.25	–
4U 1735-44	3.96	75.41 ± 0.50	<13.77	2.4 ± 1.23	<0.64	<2.06	1.96 ± 0.85	–
4U 1820-30	2.33	81.06 ± 0.10	3.48 ± 0.89	1.10 ± 0.25	<0.20	2.97 ± 0.38	1.78 ± 0.17	–
Cygnus X-2	3.09	87.95 ± 0.01	4.08 ± 0.14	1.51 ± 0.05	0.12 ± 0.01	0.72 ± 0.05	0.62 ± 0.01	–
EXO 0748-676	1.01	60.78 ± 0.14	4.59 ± 3.30	<1.65	<3.99	<1.17	<0.77	–
GRO J1655-40	7.22	48.19 ± 6.67	<2.22	<0.90	<0.23	<1.25	2.00 ± 0.51	–
GX 339-4	5.18	140.50 ± 0.11	<3.55	1.08 ± 0.25	<0.43	8.21 ± 1.17	3.19 ± 0.35	–
GX 349 + 2	6.13	<11.64	<1.73	<16.5	<0.33	<0.53	<3.33	–
GX 9 + 9	3.31	104.09 ± 0.35	6.87 ± 1.46	<1.30	<0.69	2.53 ± 0.49	1.12 ± 0.20	–
HER X-1	1.66	7.83 ± 1.42	<4.05	<0.82	<0.52	4.06 ± 2.90	<0.27	–
SER X-1	5.42	41.37 ± 0.12	<3.09	<1.42	<0.35	1.15 ± 0.57	1.62 ± 0.44	–
XTE J1817-330	2.29	78.52 ± 0.01	8.75 ± 0.03	1.23 ± 0.01	0.20 ± 0.02	1.80 ± 0.02	1.20 ± 0.02	–
Extragalactic sources								
1ES 0120 + 340	0.52	36.4 ± 0.56	<7.50	<0.82	<0.77	<0.73	<0.80	–
1ES 1028 + 511	0.12	<16.11	<5.31	<1.10	<1.97	<0.94	<2.59	–
1ES 1553 + 113	0.43	13.21 ± 0.31	1.91 ± 0.42	<0.44	<0.48	0.36 ± 0.07	<1.01	–
1ES 1927 + 654	0.92	<49.22	<6.83	<2.44	<7.78	<12.28	<1.64	–
1H0707-495	0.65	<79.53	<55.05	<23.51	<1.78	<1.97	<3.47	–
3C 382	0.92	<32.59	<16.23	<15.95	<10.67	<2.73	<7.59	$0.035^{+0.009}_{-0.007}$
3C 273	0.17	12.31 ± 0.35	2.20 ± 0.37	<0.61	<0.18	1.64 ± 0.14	0.51 ± 0.05	$0.053^{+0.003}_{-0.002}$
3C 454.3	0.65	<24.25	<10.35	<2.53	<1.42	<0.82	<3.11	–
Ark 564	0.67	18.25 ± 0.19	6.67 ± 0.48	<0.32	<0.12	<0.85	<0.53	–
B0502 + 675	1.45	<3.29	<2.77	<0.72	<1.90	<3.29	<2.49	–
H1426 + 428	0.11	33.71 ± 0.03	<5.76	<6.29	<1.61	<7.56	<3.81	–
H1821 + 643	0.34	9.79 ± 0.90	<3.64	<2.04	<0.44	<0.54	<1.03	0.030 ± 0.003
H2356-309	0.14	4.02 ± 0.71	1.37 ± 0.43	0.88 ± 0.14	0.15 ± 0.09	0.45 ± 0.08	<0.74	–
MCG-6-30-15	0.39	19.63 ± 0.65	6.62 ± 0.68	<0.82	<0.68	1.37 ± 0.17	0.92 ± 0.08	–
MR 2251-178	0.26	<15.33	<1.64	<5.62	<0.47	<2.79	<3.65	-
Mrk 279	0.17	21.57 ± 0.21	3.32 ± 0.38	1.09 ± 0.13	<0.10	0.61 ± 0.07	<0.56	0.025 ± 0.001
Mrk 1044	0.38	<25.18	5.48 ± 1.95	4.11 ± 1.56	<0.33	<3.07	<4.51	–
Mrk 421	0.20	4.93 ± 0.10	1.66 ± 0.11	<0.82	0.13 ± 0.01	0.68 ± 0.01	0.15 ± 0.02	$0.030^{+0.005}_{-0.009}$
Mrk 290	0.17	11.88 ± 3.74	<1.47	<0.79	<0.26	2.08 ± 1.05	<0.71	0.016 ± 0.006
Mrk 509	0.50	20.02 ± 0.21	<4.77	1.86 ± 0.22	<0.49	1.21 ± 0.36	<1.02	0.045 ± 0.003
NGC 3783	1.38	130.71 ± 1.78	<5.67	<2.01	<0.88	<1.12	0.53 ± 0.42	–
NGC 4051	0.11	4.64 ± 0.68	2.56 ± 0.45	<1.78	<0.63	<1.51	<3.38	–
NGC 4593	0.20	5.30 ± 1.60	<3.63	<1.02	<0.65	0.86 ± 0.35	<2.22	–
NGC 5548	0.16	6.61 ± 0.74	2.10 ± 0.72	<1.44	<0.07	<0.75	1.36 ± 0.27	0.031 ± 0.004
NGC 7469	0.52	42.86 ± 1.70	<29.26	<3.41	<0.24	<4.70	<4.91	$0.0091^{+0.0009}_{-0.0012}$
PG 1211 + 143	0.30	36.25 ± 0.07	<6.33	<6.01	<1.62	0.92 ± 0.61	<2.33	0.014 ± 0.002
PKS 2005-489	0.46	8.67 ± 2.58	<10.26	<3.31	<2.21	<0.65	<0.74	0.060 ± 0.003
PKS 2155-304	0.16	10.99 ± 0.37	2.63 ± 0.20	<0.19	<0.08	0.47 ± 0.02	0.46 ± 0.03	0.0218 ± 0.0005
Ton 1388	0.15	<21.59	10.81 ± 3.25	<2.38	<0.31	<2.72	<1.59	$0.018^{+0.001}_{-0.002}$

21 cm measurements taken from Willingale et al. (2013). *FUSE* measurements taken from Savage et al. (2003).

counts for <30 per cent of the total EW. Such contribution is not enough to solve the N(O II) and N(O VI) discrepancy. In the cases of Cygnus X–2 and XTE J1817–330, the O II Kβ-L12 accounts for ∼40 per cent of the total EW.

Fig. 3 shows the 21–24 Å wavelength region for Mrk 421, a source for which we have obtained a good constraint for both N(O II) and N(O VI). The most outstanding features associated with oxygen X-ray absorption in the ISM are also indicated. We tried to model the absorption line located at ∼22.04 Å by fixing the N(O VI) in the `IGMabs` model to the *FUSE* measurement and increasing the N(O II) until we obtain low residuals around the line wavelength position. We found that this resulted in worse-fit statistics because when assuming the *FUSE* N(O VI) a larger amount of O II is required to model the ∼22.04 Å line, overestimating the strengths of other lines, in particular the O II Kα, located at 23.35 Å. Fig. 3 also included the data/model ratios obtained for those sources for which *FUSE* measurements are available when applying the same procedure. As before, the residuals around the O II K α absorption line increase as we increase the N(O II). In all cases, the statistics is worse by $\Delta\chi^2 > 15$, except for NGC 7469 ($\Delta\chi^2 = 8$) and Ton 1388 ($\Delta\chi^2 = 6$). These results indicate that the blending of O VI K α and the O II K β-L12 absorption features is not sufficient to account for the discrepancy between X-ray and UV measurements.

Other possibilities to explain the O VI mismatch between UV and X-ray measurements include the atomic data calculation, saturation of the lines, and radiative excitation. In the case of O II, given that the Auger widths tend to be larger than the radiative widths (García et al. 2005), it is crucial to include such effect, which can lead to an increasing of the EW up to 50 per cent for a fixed column density. However, it is not trivial to compute all

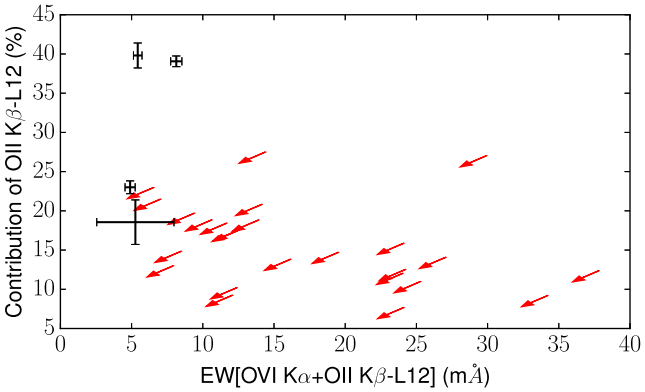

Figure 2. Percentage contribution of the O II K β-L12 line to the total (O II K β-L12 + O VI K α) EW. Black points are for sources where both O II K β-L12 and O VI K α are measured. Red arrows are for sources where the two lines have only upper limits.

the multiple channels for the Auger decay of the K vacancy states, making difficult to estimate accurately the Auger damping. Also, as was noted by Bizau et al. (2015), there is a discrepancy between the theoretical and experimental values for the oscillator strengths and line width for O II Kβ-L12, which has not been addressed. In the case of saturated lines, given the dependence of the EW with the broadening velocity $v_{\rm turb}$, there is a N(O VI)-$v_{\rm turb}$ degeneracy which can lead to under(over)estimation of the column density (up to one of magnitude for $v_{\rm turb} > 200\,{\rm km\ s^{-1}}$, see Draine 2011; Nicastro et al. 2016a). UV data provides a good constraint on the velocity because multiple transitions of the same ion can be modelled simultaneously, thus allowing the disentangling of such degeneracy (Savage & Lehner 2006; Bowen et al. 2008). However, even when the $v_{\rm turb}$ value assumed in our model is within the broadening velocity found in UV studies (see, for example, Savage & Lehner 2006) the mismatch between the column densities remains. With respect to radiative excitation, as mentioned by Arav et al. (2003), electron impact excitation and recombination may contribute to the O VI emission, reducing the absorption from the ground state. But such effect can only account for one-half factor of difference between UV and X-ray, much lower than the discrepancy observed (Mathur et al. 2017).

4 CONCLUSIONS

We have analysed the oxygen edge absorption region (18–24 Å) using high-resolution X-ray spectra from 13 LMXBs and 29 extragalactic sources. Using the `IGMabs` model, we have estimated column densities, ion by ion, required to fit all the absorption signatures in the spectra. We have focused the analysis in the estimation of N(O VI), which can be difficult due to contamination by the O II K β-L12 absorption feature at 22.04 Å located close to the O VI K α absorption line at 22.032 Å. N(O VI) was constrained for two Galactic and two extragalactic sources from our sample. For the rest of the sources, we report upper limits. We have found that for low N(O II), the N(O VI) contribution is larger, a hint of the blending between the line. However, this blending cannot be the entire solution for the discrepancy between X-ray and UV measurements of N(O VI). Other possibilities include atomic data calculation, saturation of the lines, and radiative excitation; however, they cannot completely solve the UV/X-ray discrepancy neither, which remains as an open question. Finally, our findings highlight the need for an accurate modelling of the absorption features associated to the local ISM

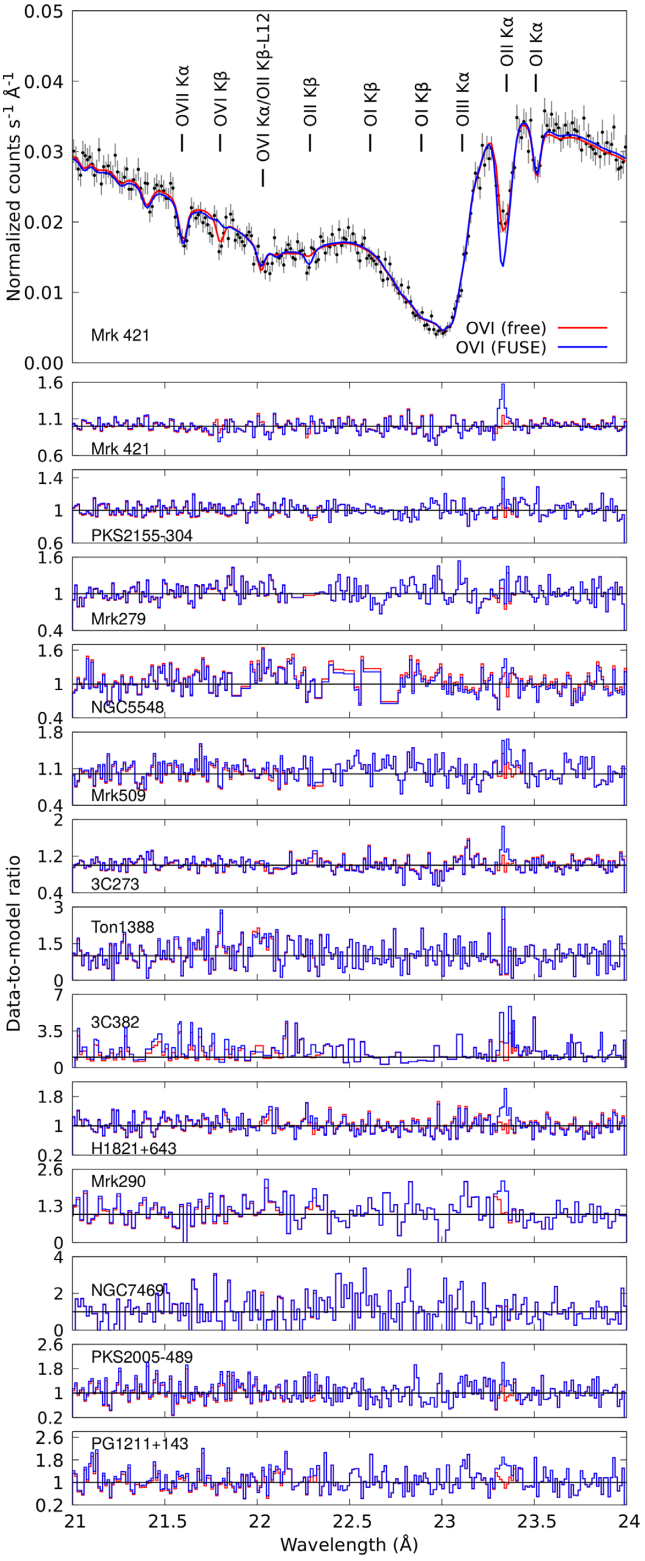

Figure 3. Oxygen edge absorption region for those sources in the sample that have both X-ray and UV column density measurements. Red solid lines correspond to the best-fit model obtained when N(O VI) is a free parameter (see Table 1). Blue solid lines correspond to the fit obtained by fixing N(O VI) to *FUSE* value and increasing N(O II) until modelling the ∼22.04 Å absorption line.

before searching for lines associated to other absorbers, including the warm–hot intergalactic medium, ultraluminous X-ray sources, active galactic nucleus, and X-ray binaries, which constitute key science goals for future missions such as *Arcus* and *Athena*.

ACKNOWLEDGEMENTS

This research was supported by the Deutsche Forschungsgemeinschaft (German Research Foundation, DFG) cluster of excellence 'Origin and Structure of the Universe'. E.G. thank Amit Pathak, Ken Sembach, and Bart Wakker for helpful comments on the UV absorption line measurements. J.A.G. acknowledges support from the National Aeronautics and Space Administration (NASA) grant 80NSSC17K0345 and from the Alexander von Humboldt Foundation.

REFERENCES

Anderson L. D., Armentrout W. P., Johnstone B. M., Bania T. M., Balser D. S., Wenger T. V., Cunningham V., 2015, ApJS, 221, 26
Arav N., Kaastra J., Steenbrugge K., Brinkman B., Edelson R., Korista K. T., de Kool M., 2003, ApJ, 590, 174
Arcodia R., Campana S., Salvaterra R., Ghisellini G., 2018, A&A, 616, A170
Bailey M., van Loon J. T., Sarre P. J., Beckman J. E., 2015, MNRAS, 454, 4013
Bizau J. M., Cubaynes D., Guilbaud S., Al Shorman M. M., Gharaibeh M. F., Ababneh I. Q., Blancard C., McLaughlin B. M., 2015, Phys. Rev. A, 92, 023401
Bowen D. V. et al., 2008, ApJS, 176, 59
Brandt T. D., Draine B. T., 2012, ApJ, 744, 129
Churazov E., Gilfanov M., Forman W., Jones C., 1996, ApJ, 471, 673
Draine B. T., 2011, Physics of the Interstellar and Intergalactic Medium, Princeton Univ. Press, Princeton Univ. Press
den Herder J. W. et al., 2001, A&A, 365, L7
Faerman Y., Sternberg A., McKee C. F., 2017, ApJ, 835, 52
García J., Mendoza C., Bautista M. A., Gorczyca T. W., Kallman T. R., Palmeri P., 2005, ApJS, 158, 68
García P., Bronfman L., Nyman L.-Å., Dame T. M., Luna A., 2014, ApJS, 212, 2
Gatuzz E., Churazov E., 2018, MNRAS, 474, 696
Gatuzz E. et al., 2013, ApJ, 768, 60
Gatuzz E., García J., Mendoza C., Kallman T. R., Bautista M. A., Gorczyca T. W., 2014, ApJ, 790, 131
Gatuzz E., García J., Kallman T. R., Mendoza C., Gorczyca T. W., 2015, ApJ, 800, 29
Gatuzz E., García J. A., Kallman T. R., Mendoza C., 2016, A&A, 588, A111
Gatuzz E., Ness J.-U., Gorczyca T. W., Hasoglu M. F., Kallman T. R., García J. A., 2018, MNRAS, 479, 2457
Giannetti A., Wyrowski F., Leurini S., Urquhart J., Csengeri T., Menten K. M., Bronfman L., van der Tak F. F. S., 2015, A&A, 580, L7
Jackson J. M., Finn S. C., Rathborne J. M., Chambers E. T., Simon R., 2008, ApJ, 680, 349
Juett A. M., Schulz N. S., Chakrabarty D., 2004, ApJ, 612, 308
Juett A. M., Schulz N. S., Chakrabarty D., Gorczyca T. W., 2006, ApJ, 648, 1066
Kalberla P. M. W., Burton W. B., Hartmann D., Arnal E. M., Bajaja E., Morras R., Pöppel W. G. L., 2005, A&A, 440, 775
Mathur S., Nicastro F., Gupta A., Krongold Y., McLaughlin B. M., Brickhouse N., Pradhan A., 2017, ApJ, 851, L7
McLaughlin B. M. et al., 2017, MNRAS, 465, 4690
McQuinn M., 2016, ARA&A, 54, 313
Miller M. J., Bregman J. N., 2015, ApJ, 800, 14
Moss V. A., Lockman F. J., McClure-Griffiths N. M., 2017, ApJ, 834, 155
Nicastro F., Senatore F., Gupta A., Guainazzi M., Mathur S., Krongold Y., Elvis M., Piro L., 2016a, MNRAS, 457, 676
Nicastro F., Senatore F., Krongold Y., Mathur S., Elvis M., 2016b, ApJ, 828, L12
Pathak A., Pradhan A. C., Sujatha N. V., Murthy J., 2011, MNRAS, 412, 1105
Pradhan A. K., 2000, ApJ, 545, L165
Sarma R., Pathak A., Murthy J., Sarma J. K., 2017, MNRAS, 464, 4927
Savage B. D., Lehner N., 2006, ApJS, 162, 134
Savage B. D. et al., 2003, ApJS, 146, 125
Savage B. D. et al., 2017, ApJS, 232, 25
Schlafly E. F. et al., 2016, ApJ, 821, 78
Shull J. M., Smith B. D., Danforth C. W., 2012, ApJ, 759, 23
Wakker B. P., Savage B. D., Fox A. J., Benjamin R. A., Shapiro P. R., 2012, ApJ, 749, 157
Welsh B. Y., Lallement R., Vergely J. L., Raimond S., 2010, A&A, 510, A54
Willingale R., Starling R. L. C., Beardmore A. P., Tanvir N. R., O'Brien P. T., 2013, MNRAS, 431, 394
Xue M., Jiang B. W., Gao J., Liu J., Wang S., Li A., 2016, ApJS, 224, 23

This paper has been typeset from a TEX/LATEX file prepared by the author.